Stress corrosion cracking detection using non-contact ultrasonic techniques

F. Hernandez-Valle, A.R. Clough, R.S. Edwards*

Department of Physics, University of Warwick, Coventry, CV4 7AL, UK

Abstract

In this work a method is presented for detecting and locating stress corrosion cracking (SCC) in stainless steel pipe samples. The method combines laser generation and either laser or electromagnetic acoustic transducer (EMAT) detection, scanning the generation point across the sample surface. Using laser-generated ultrasonic waves that interact with the cracks, and performing time-frequency analysis techniques to examine changes in the generated wavemodes, surface plots that clearly resolve the spatial extent and geometric alignment of the cracks are created and presented here. The method is demonstrated using components removed from service after exhibiting SCC.

Key words: Stress corrosion, stainless steel, Ultrasonics, Nondestructive testing, Time-frequency analysis

1. Introduction

The interaction of a corrosive environment and tensile stress (e.g. directly applied stresses or in the form of residual stresses) can produce failure in the form of stress corrosion cracking (SCC) in susceptible metallic components [1]. The damage produced by SCC is not always obvious to casual inspection, so failure can be both unexpected and catastrophic. Thus, early detection of such defects is important in order to have sufficient time for adequate measures to be taken, for example repair or replacement of the damaged component.

*Corresponding author

Email address: r.s.edwards@warwick.ac.uk (R.S. Edwards)

Various nondestructive evaluation (NDE) techniques have been trialled to detect and locate this type of cracking, all with certain advantages and disadvantages. For example, dye penetrant testing is a widely used and relatively simple method which can be easily performed at remote test sites. However, besides requiring surface preparation, dye penetrant can only detect defects that are open at the sample surface, and it performs poorly on hot, dirty, and rough surfaces as well as on porous materials [2, 3]. Eddy current and pulsed eddy current techniques can be used for rapid inspection, and have a relatively small probe size, and there is no need to physically contact the test samples. However, eddy current inspection only detects surface or near-surface defects, it is very sensitive to a wide range of parameters related to the conductivity and magnetic permeability of the test sample, and is very sensitive to lift-off variations [4–6].

Radiographic inspection has the advantage over many other NDE techniques in that analysis and interpretation is almost intuitive. Amongst radiographic methods, X-ray tomography excels where information is needed in three spatial dimensions [7–9]. However, despite the advantages, radiation techniques have serious safety concerns due to possible overexposure to large amounts of radiation. In addition, a closed crack will generally only be detectable in a radiograph at certain orientations, ideally when the long dimension of the crack is parallel to the direction of radiation propagation [7–9].

Various ultrasonic techniques have been used for SCC detection, in particular time of flight diffraction (TOFD). This technique relies on the detection of weak diffracted waves arising at the edges or tip of a crack, and can locate and size defects either within the bulk of a sample, or on the surface [10, 11]. Although TOFD is well understood and widely used it has some limitations, such as the assumption that there is no interference from other wavemodes. In some geometries this will limit its applicability to cases where there is only a single defect, thus research to add new features and remove some limitations is still being performed [10, 11].

Standard ultrasonic measurements, particularly those looking for reflections of bulk waves from defects, have difficulties due to the low reflection and transmission coefficients for closed and partially closed defects. However, recent work looking at the interaction of

surface waves with surface-breaking defects in the near-field have shown several enhancement mechanisms which can be used for identification of cracking [12–20]. For Rayleigh wave propagation on thick samples, the signal enhancement observed when scanning the detector across the crack is due to the constructive interference of incident, reflected and mode-converted waves [12, 13, 15]. For defects propagating at an angle to the surface, where the local thickness changes throughout the defect, further large enhancements are also seen in the time and frequency domains [21–23]. Similar effects are seen when scanning thin samples using Lamb waves, with enhancements observed as an increase in magnitude of the signal at certain frequencies [24]. These distinctive features can be used to identify the defect and give some information about its geometry [23].

For laser generation, further enhancement effects have been observed due to the changes in generation conditions when the generation spot is over a defect [18–20, 25]. As the laser spot passes over the defect, the boundary conditions of generation on the surface will change, and this has been shown to give an increase in the magnitude of the signal at certain frequencies. If the defect is partially closed and the laser spot source is directly illuminating the defect, then the material will also undergo thermo-optic crack closure, which has been shown to produce higher order frequency components [20].

In this paper we examine the near-field interactions of laser generated ultrasonic waves with stress corrosion cracking in stainless steel pipe samples removed from service, and use the ultrasonic signal enhancement to resolve the spatial extent and geometric alignment of those cracks. Ultrasonic waves generated in bounded media, such as pipes, take the form of guided waves. These travel along the pipe with different propagation and displacement behaviour depending on the particular wavemode (e.g. longitudinal, torsional or flexural modes in pipes, and higher-orders of each of these) [26]. The particular wavemodes generated depend on the pipe geometry, the material, the generation source used and also the testing frequency. Quantification of the enhancement effect for guided waves in the time domain is complicated due to the presence in most cases of more than one wavemode, thus time-frequency analysis is performed in order to highlight which modes were generated and/or enhanced [19].

The generation of ultrasound here was performed using a thermoelastic laser source, described in section 2. For detection two different approaches were used; laser interferometry techniques (section 3.1) or electromagnetic acoustic transducers (EMATs, section 3.2). Both approaches are non-contact, and hence their influence on the sample properties and on the wavemode being measured is negligible [27]. Both can easily be scanned across the sample surface, and can work on rough surfaces and in hostile environments. Laser detection has the advantage of high spatial resolution, which adds to the accuracy of defect location. However, laser detection systems are still a costly option when compared to the EMAT detection approach.

The paper is organised as follows. In section 2, a description of the experimental setup and time-frequency analysis are given. Results from scans of damaged pipe samples and discussion of each detection approach are given in sections 3.1 and 3.2. Finally, a summary of the uses of these approaches is presented in section 4.

2. Experimental method

Experiments were performed using a pulsed Nd:YAG laser (1064 nm wavelength and 10 ns pulse duration) to generate ultrasound, focused into a point of approximately 500 μm diameter. The laser was filtered such that it acted in the thermoelastic regime, minimising damage to the sample, to generate broadband ultrasonic waves [28]. In this regime, the area impinged by the laser beam is heated rapidly, expanding and generating stress as the surrounding cooler material constrains its expansion. The associated pulse of material expansion and contraction can generate a range of ultrasonic modes, such as bulk longitudinal and shear waves, or Rayleigh waves and other guided wave modes, depending on the sample geometry. For detection, to investigate the near-field interactions of surface acoustic waves with SCC, two different approaches were used; laser detection, or EMATs [27].

For laser detection, a two-wave mixer laser interferometer system from Intelligent Optical Systems [29] was used (setup shown in figure 1a). The interferometer is sensitive to the out-of-plane component of the surface displacement, and has a bandwidth of 125 MHz, allowing

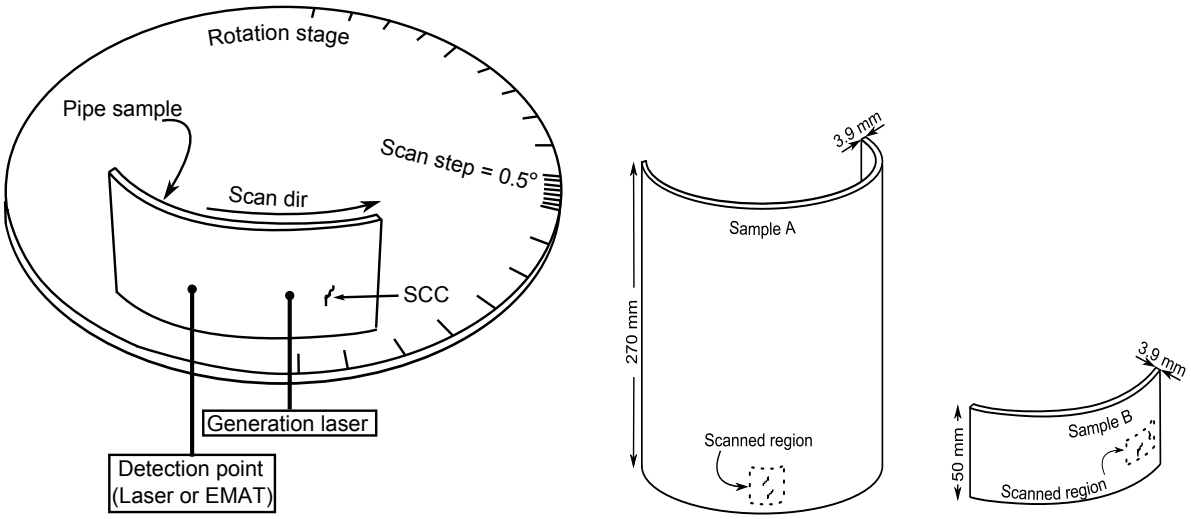

(a) Set-up (b) Pipe samples

Figure 1: Experimental setup used for inspection of stainless steel pipes containing SCC for laser or EMAT detection (a). Dimensions and scanned regions of both samples are shown in (b), with a schematic of the orientation of the measured defects relative to the pipe.

measurements over a wide range of frequencies. Its continuous wave laser (200 μm spot-size) operates at 1550 nm, with a power variable up to 2 W; this is varied depending on the sample surface quality. The interferometer works on rough surfaces without the need for surface preparation. [29]

For EMAT measurements, linear detection coils were used, produced by wrapping 10 turns of 0.08 mm diameter insulated copper wire around NdFeB magnets of field approximately 0.5 T, with the field aligned either into the sample, for measuring predominantly in-plane particle velocity, or along the sample surface for measuring predominantly out-of-plane velocity. The transducer active measurement area was 1 mm (width) by 35 mm (length). For a description of the principle of operation and more detailed description of the EMATs used, the reader is referred to reference [23].

Measurements presented here were done on two different AISI 304 stainless steel sections of pipes removed from service. Both pipe sections had an inner diameter of 152.4 mm and an outer diameter of 160.2 mm, and hence a wall thickness of 3.9 mm, with different axial

lengths; 270 mm (sample A) and 50 mm (sample B, see figure 1b). Sample A contained two cracks (SCC 1 & SCC 2) and some pitting damage in the region of interest (figure 4a), whereas sample B contained several features which looked like surface-breaking cracks to visual inspection (figure 5a).

Regardless of the detection technique, the scanning process consisted of placing each sample on a rotational stage to perform a circumferential scan, such that the generation laser source passed over the region of interest with constant steps; these increments correspond to the x-axis on the surface plots shown in figures 4, 5, and 10. The vertical position of the generation and detection points was then varied, starting from the lowest part of the region of interest and moving up until reaching the upper part with increments of approximately 2 mm; these increments correspond to the y-axis on the surface plots.

Guided ultrasonic wave modes were generated, propagated along the sample, and were detected by the laser or EMAT. Since guided waves in pipes can consist of several different wavemodes, with those present depending on the pipe geometry, the frequency of the ultrasonic wave and the generation source [26], mode identification using just the signals in the time domain is complicated. For this reason, a time-frequency analysis was performed on each A-Scan at each scan point to identify the arrival time of each frequency component, and to highlight which modes were generated and/or enhanced (see figures 2, 6 and 7) [19, 24, 30]. Each wavemode has a frequency-dependent velocity which can be calculated, and hence the sonogram analysis used here is able to identify modes based on their arrival times, and allow identification of modes which show sensitivity to the presence of a surface-breaking defect. An increase in the magnitudes of these modes at a defect can then be measured through windowing the correct region of the sonogram, and used for the construction of surface plots that resolve the spatial extent and geometric alignment of SCC in the pipe's surface.

3. Results and discussion

3.1. Laser-Laser SCC measurements

For measurements using the laser-laser system, the laser spot source and laser detector were scanned circumferentially around the pipe section in increments of 0.5° (scan step of

approximately 0.67 mm) with a fixed circumferential separation, such that the spot source passed over the defect region, as shown in figure 1a. To identify the arrival time of a specific mode at a chosen frequency a sonogram was produced at each scan position [19, 24, 30]. For positions at which the source was located far away from the defect a low frequency surface acoustic wave was observed, and was used as representative data for a defect free region of the pipe; an example of this is shown in figure 2a. The bottom part of this figure shows the A-Scan, with the top part of the figure the frequency content at each time. Primarily low frequency modes are generated, and the measurement is sensitive to out-of-plane motion, hence will only be sensitive to certain wavemodes [26]. For positions when the source is fully illuminating the defect a high frequency enhancement can be observed, in the form of the extra wavemode shown in figure 2b, which is accompanied by a visible change in the A-Scan at the source location. The sharp wave at about 18-20 μs is the wavemode shown by the near-vertical line on the sonogram.

As can be seen on the A-Scans in figure 2, analysis in the time domain of these signals is complicated, and the amplitude measurements used when studying enhancements of Rayleigh waves are not easily applicable [15]. However, this high frequency enhancement is very similar to that observed when Lamb waves are generated at defects on thin, flat plates, which is due to the generation of new mode converted waves at the defect, and the change in the boundary conditions of generation that occurs as the laser source passes over the defect [18, 19, 24, 25]. This is analysed by studying magnitude variations in selected regions of the sonogram. To quantify the enhancement for this data, the peak magnitude in the sonogram data (maximum value of the z-component) of two regions of the sonogram were recorded across the duration of the scan, chosen based on knowledge of the relevant dispersion curves [26], and on the regions which were observed to show the most significant changes during the scan. The first region was bounded by the frequency range between 1-2 MHz and arrival times of 17.14-20.14 μs, with the variation in the magnitude as a function of scan position shown in figure 3a. This shows an increase at the defect but also some variation at other positions. The second region was at a higher frequency range of 2 - 3 MHz, arriving between 18.54 and 20.54 μs, with the variation in the magnitude as a function of

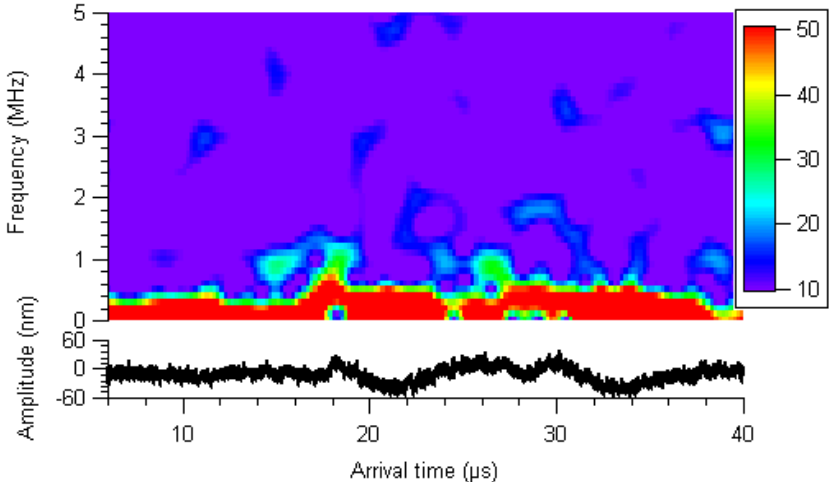

(a) Reference

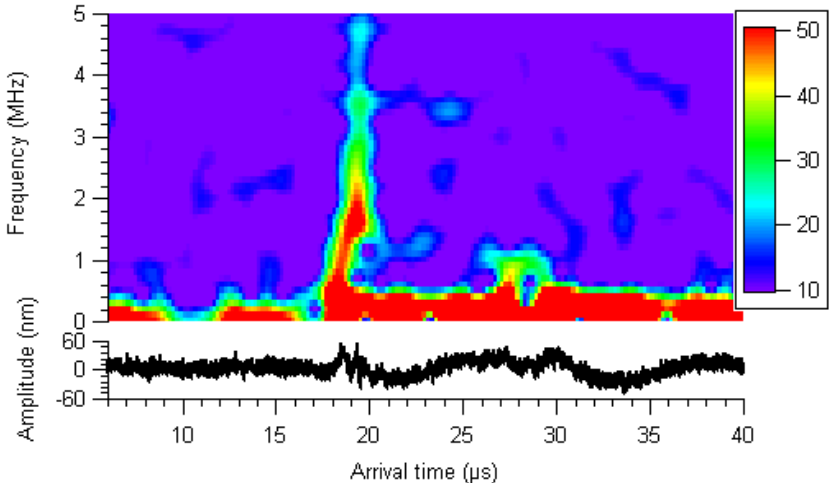

(b) Enhanced

Figure 2: Sonograms with and without defect present for the laser source passing over defect region.

scan position shown in figure 3b.

Both of these analysis regions show a clear increase in peak magnitude in the chosen regions at the position of a known defect, along with variations at other positions. In order to improve the probability of detection (PoD) of the SCC and have a clear image of the true extent of the defects, the product of the two sets of peak magnitude data was used. This is shown in figure 3c, and clear peaks in the magnitude are observed for positions at which the source illuminates the defect, with the magnitude returning to a steady lower level in regions free from surface defects.

The generation and detection points were scanned across the sample, as described in section 2, producing a figure similar to figure 3c for each vertical position. The magnitude data for each scan were then stacked next to each another to form a surface plot of the enhancement behaviour across the sample, shown in figure 4b. Here, the colour scale represents the extent of the enhancement in each scan as a function of the source position, with the lighter areas corresponding to larger magnitudes, and dark areas to magnitudes below a chosen threshold based on the 'no-defect' magnitude. A photograph of the scanned area (figure 4a) shows two stress corrosion defects, labelled SCC1 and SCC2, and several instances of smaller patches of pitting damage. In the enhancement surface plot in figure 4b, the two defects can be clearly resolved with their spatial extent and geometric alignment identifiable from the image. Two instances of the pitting damage can also be observed in the upper left hand corner of the surface image as bright spots. The spatial extent of these defects is smaller than the two stress corrosion cracks and this is reflected in their small spatial extent in the surface plot; resolution could be improved significantly by using smaller scan steps.

The image in figure 4b highlights the advantages of the near-field inspection method for the resolution of multiple partially closed surface defects in close proximity, with several defects successfully resolved. A far-field inspection technique based on reflection or transmission from the defects would show little evidence of their presence due to the low reflection and high transmission of the incident wave at the defects, illustrated by the lack of any significant change in the waveform when the defect lies between the source and detector. The low reflectivity prevents a pulse-echo investigative approach, and the high transmission

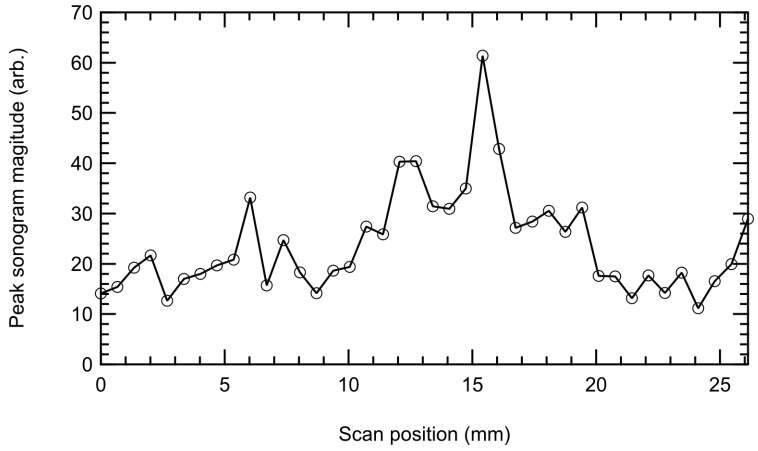

(a) Low frequency

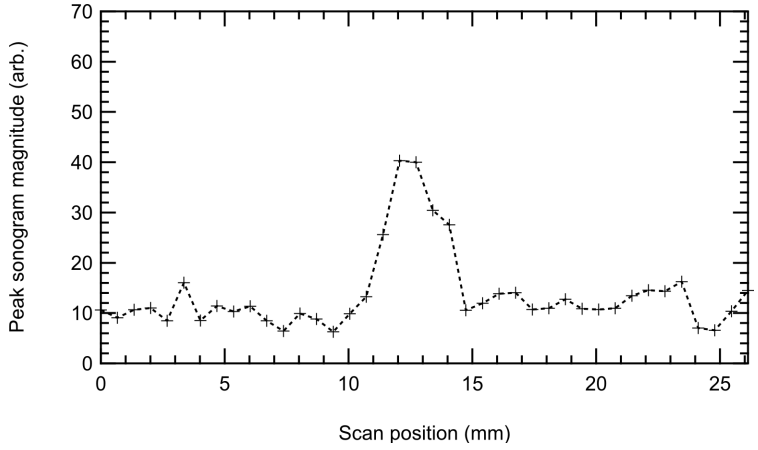

(b) High frequency

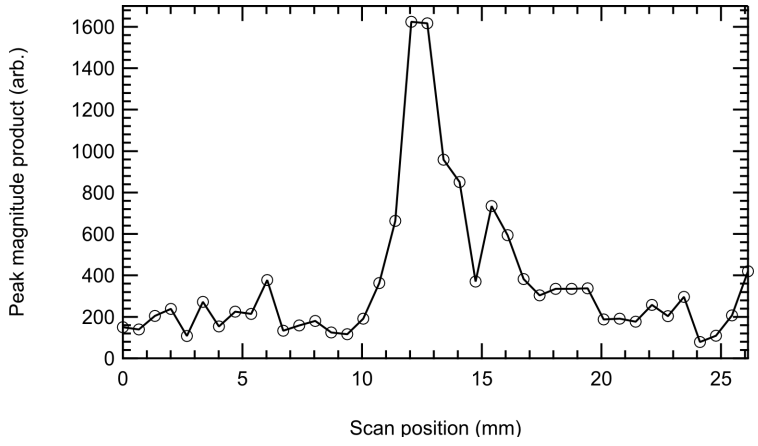

(c) Product

Figure 3: Peak sonogram magnitudes for low (a) and high (b) frequency regions, allowing the production of an improved PoD by taking the product of the two (c).

makes it challenging to resolve the defect through changes in the transmitted waves.

The photograph of sample B (figure 5a) shows several marks, each of which could be indicative of cracking. However, the image produced from the signal enhancements in figure 5b shows clearly that there are two partially closed defects with a small separation, close to the sample edge. These enhancements from defects are distinct from the enhancement arising as the spot passes over the edge of the sample (right hand side of the figure), which also shows enhancement similar to a full thickness defect across the width of the sample. Closer inspection of the defect area in figure 5a showed that the apparent defect located in the upper left of the image was in fact dirt on the sample surface. The fact that no signal enhancement was seen as the source passed over this region illustrates the effectiveness of the technique for distinguishing real defects from damage which may falsely be identified by visual testing. The surface plot in figure 5b highlights the advantages of the laser-laser near-field approach used here.

3.2. Laser-EMAT SCC measurements

Whilst the laser-laser system has many advantages, including the excellent spatial and frequency resolution, the high cost of such a system means that it is not always practical for use. Furthermore, certain wavemodes will have only a small amplitude in the out-of-plane direction, and a significant in-plane motion [26]. EMATs may prove to be a suitable inexpensive detection alternative, with the capability to detect in-plane or out-of-plane motion [23].

In a similar fashion to the laser-laser approach, the laser spot source was scanned circumferentially in increments of 0.8° (scan step of approximately 1 mm) such that the spot source passed over the defect region, but with detection using an EMAT. To simplify the experimental procedure the EMAT was held fixed in the same position on the sample, and hence the circumferential separation between generation and detection points increased when the rotational stage was moved. Two different EMAT configurations were tested, one of which was sensitive to the out-of-plane (OP) particle velocity, and other sensitive to the in-plane (IP) particle velocity [23, 27], allowing sensitivity to different wavemodes [26, 31].

In order to identify the arrival times and frequency components of surface acoustic waves

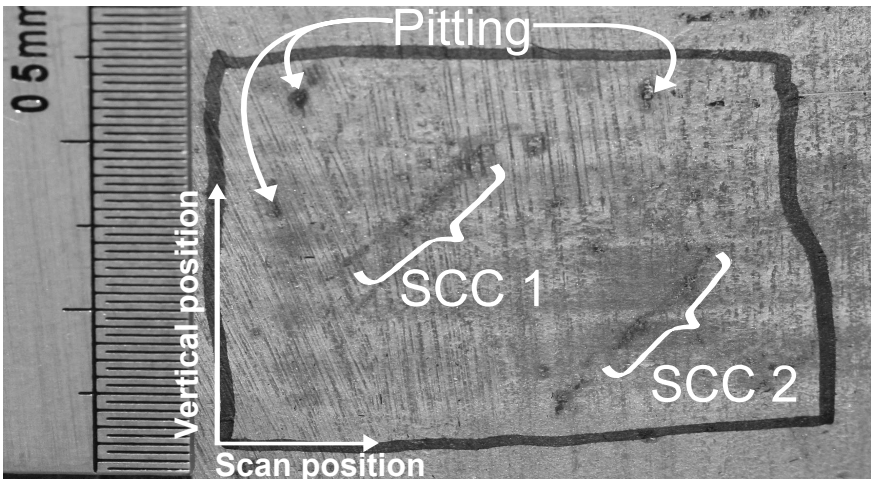

(a) Sample A

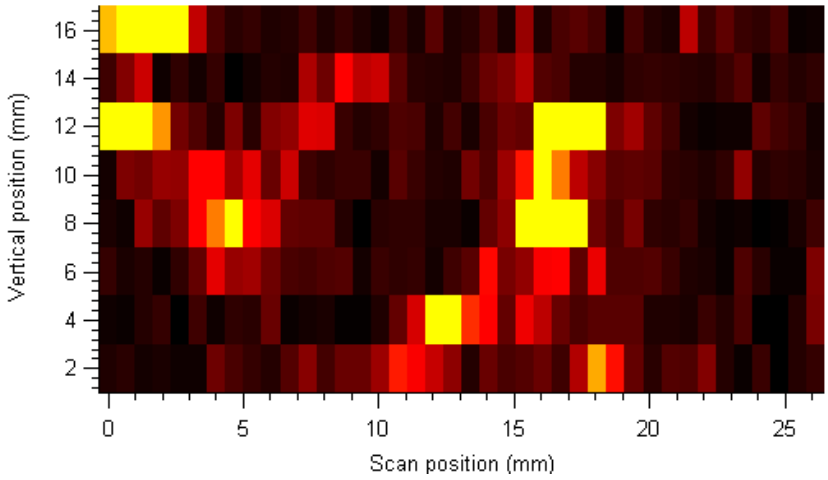

(b) Surface map

Figure 4: Close-up of the region containing SCC in sample A (a), and surface plot showing enhancement of the surface acoustic wave generated through interaction of the laser spot source with defects (b).

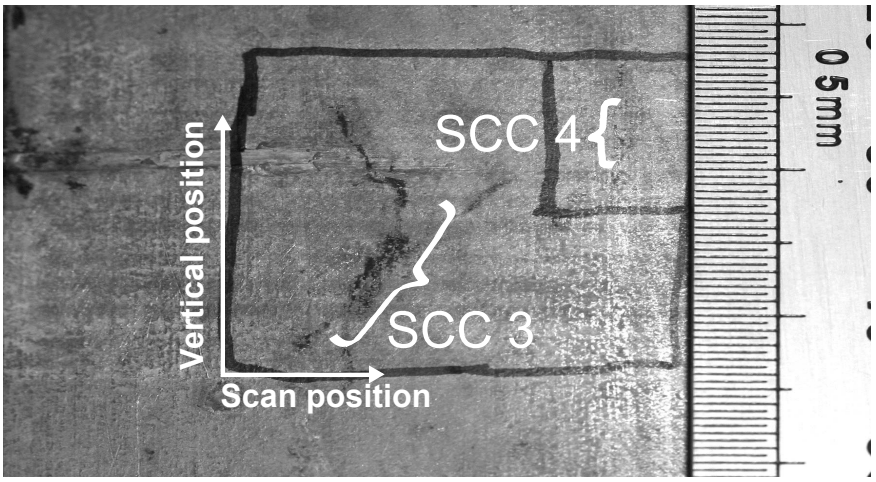

(a) Sample B

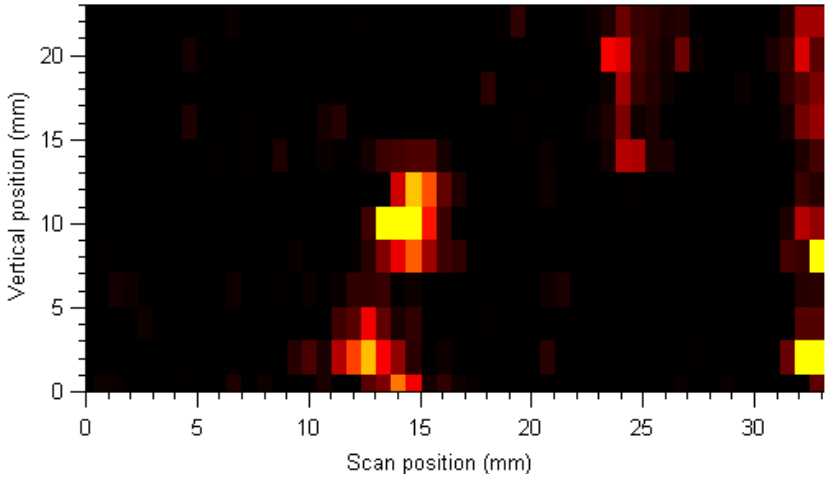

(b) Surface map

Figure 5: Close-up of the region containing SCC in sample B, and 2D surface plot showing the surface wave enhancements with multiple defects and edge enhancements visible.

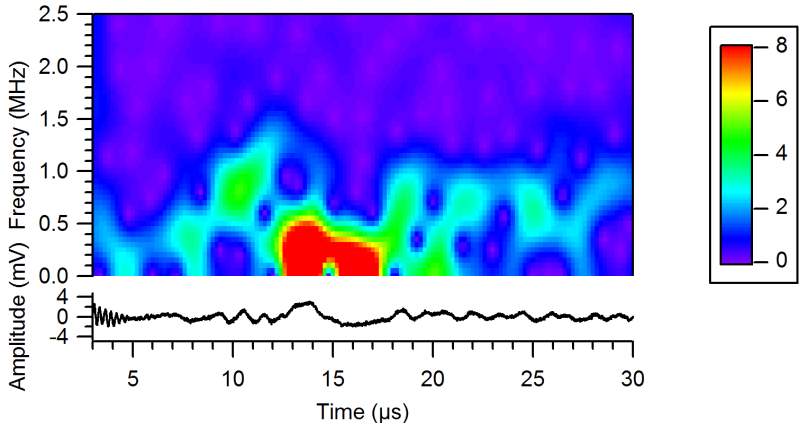

(a) Reference - OP

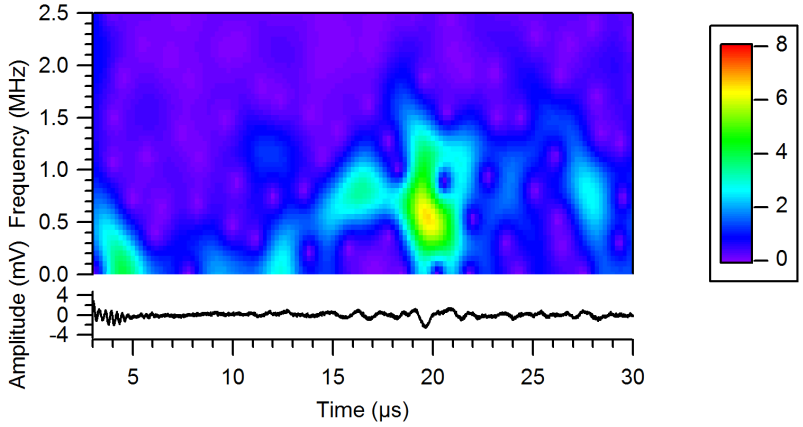

(b) Enhanced - OP

Figure 6: Sonograms for scan positions where the laser is far away (a) and fully illuminating (b) the defect region; detecting with an EMAT sensitive to out-of-plane velocity.

a sonogram was again produced for each A-scan obtained using either the in-plane or out-of-plane EMAT. Positions at which the laser source was located far away from the defect were again considered as representative of a defect-free region of the pipe, and are shown for the out-of-plane and in-plane cases in figures 6a and 7a respectively. For positions where the laser source was fully illuminating the defect, extra signals at higher frequencies accompanied by a visible change in the A-scan can also be observed in both cases (see figures 6b and 7b).

There are some differences between the data shown in figures 6 and 7, and that in figure 2 for laser-laser measurements. The EMAT measurements are made with a varying

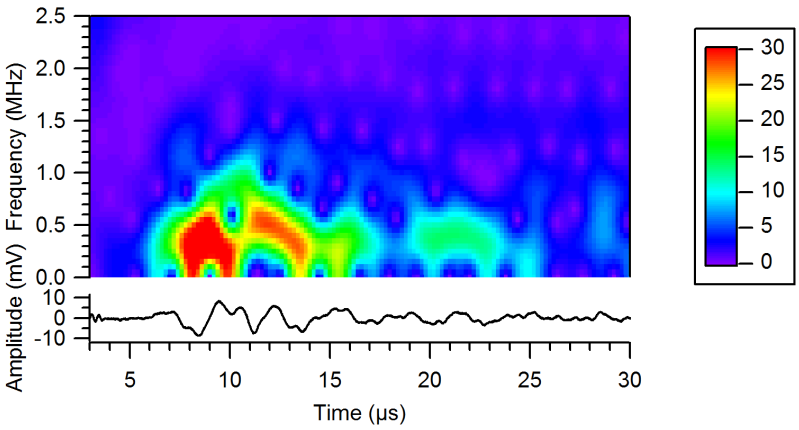

(a) Reference - IP

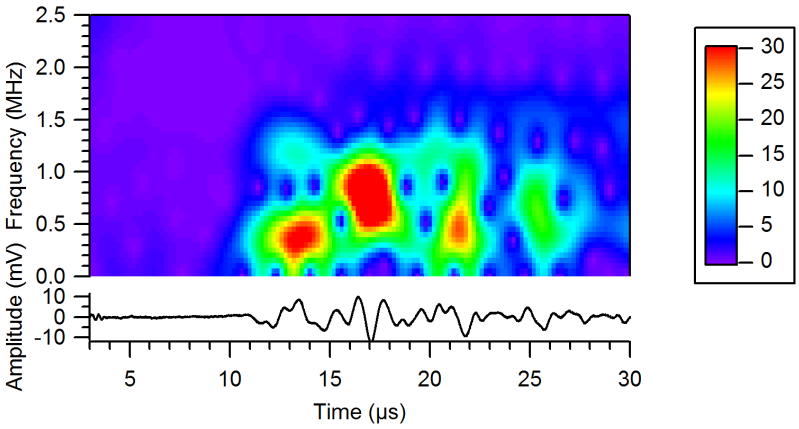

(b) Enhanced - IP

Figure 7: Sonograms for scan positions where the laser is far away (a) and fully illuminating (b) the defect region; detecting with an EMAT sensitive to in-plane velocity.

separation between generation and detection points, and hence the wavemodes will arrive at different times during the scan. The EMATs also measure particle velocity rather than surface displacement. Finally, the expected differences between the wavemodes detected in the in-plane and out-of-plane velocity components is clear [26].

The determination of the frequency ranges for analysis is more complicated for the EMAT results, given the varying arrival time and the lower signal to noise ratio. The choice of frequency range must consider the particle velocity sensor nature of the EMATs, and the bandwidth limitations due to the coil width [32, 33]. The coil used in both EMATs has a narrow but finite width, in this case approximately 1 mm. When the width of the coil becomes comparable to the wavelength of the wave passing underneath the coil, the acquired signal will not be a true representation of the particle velocity in the sample associated with the wave propagation [31]. This effect is known as the spatial impulse response, and it has been shown that the EMAT response for wavelengths less than one half of the coil width will fall below 10% of the amplitude for the long wavelength limit [31], as shown in figure 8 (figure produced following the model presented in [31] for a sinusoidally varying wave). This means that the EMATs used here will not detect significant signal amplitude for signals of less than 1 mm wavelength (corresponding to a frequency of 3 MHz), and for wavelengths around this value there will be resonant effects.

Once the regions of enhancement have been identified, avoiding regions where the frequency is close to a minimum in the EMAT response, the same procedure to quantify the enhancements as for the laser-laser measurements was used. The peak magnitudes in two regions on the sonograms were tracked; the first of which was at 0.5-1 MHz and the second at 1-2 MHz, with a window length of 4μs, with the window moved in time to match the mode arrival time due to the increasing separation between generation and detection points. The peak magnitudes for the low and high frequency regions are shown in figures 9a and 9b, for out-of-plane and in-plane velocities respectively.

As with the laser-laser measurements, both figures show some peaks and troughs, but the exact enhancement region is not completely clear from each plot individually. Hence the product of the peak magnitudes for both regions was again taken to improve the PoD.

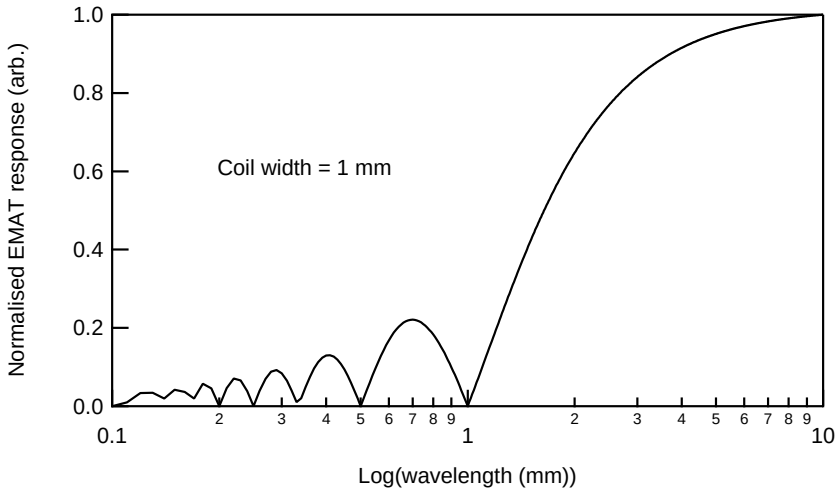

Figure 8: EMAT response as a function of wavelength for a sinusoidally varying wave as the wavelength is varied. The first minima occurs when the coil width is equal to the wavelength.

In this case, the signals were still noisy with a low PoD, and the out-of-plane and in-plane products were also combined, as the presence of a defect should have some effect on both. By obtaining the product of all four peak magnitudes a surface map was constructed. This is shown in figure 10, and again the two defects were resolved (note that the scanned region was not exactly the same as for the laser-laser measurements, and hence the pitting damage is not shown).

4. Conclusions

When defects are partially closed and a laser is used to generate ultrasound, for the laser spot source directly illuminating the defect the thermo-optic crack closure changes the generation conditions for the ultrasound and also alters the reflection and transmission behaviour of the defect. This produces the higher order frequency components observed here which have been used to track enhancements of the signal [20, 25]. The surface images produced from the scans of the samples can be used to identify defects, either by visual inspection of the data produced by the time-frequency analysis, or through automated identification using suitable software [34].

Laser generation combined with detection using either laser interferometry or EMATs

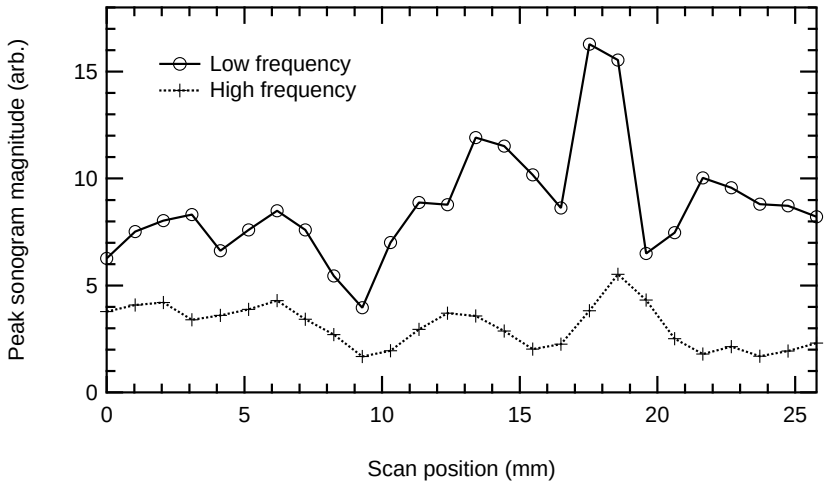

(a) OP

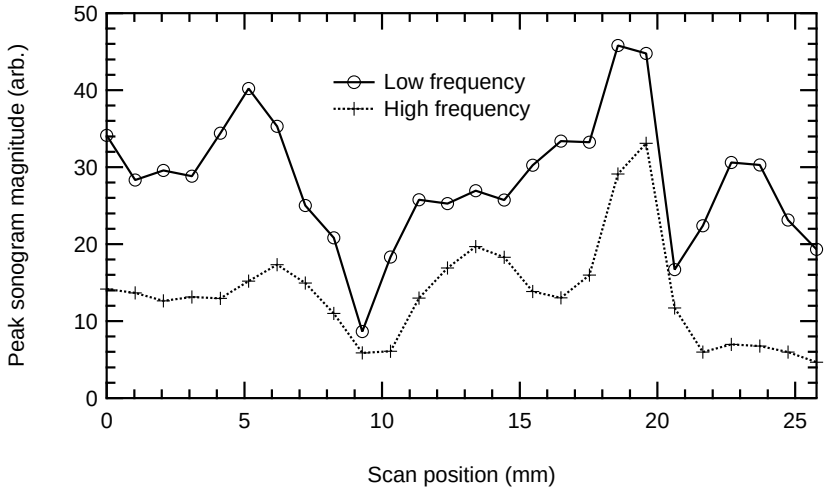

(b) IP

Figure 9: Peak sonogram magnitudes for low and high frequency regions, detecting with an EMAT sensitive to OP particle velocity (a), or IP particle velocity (b).

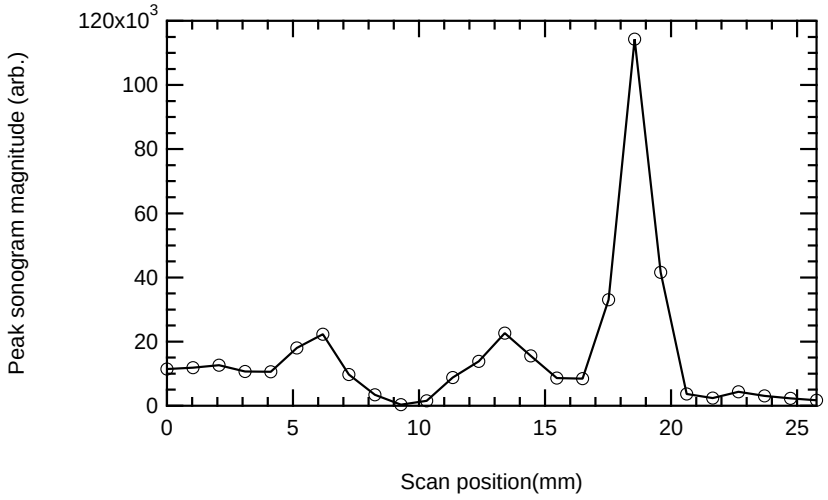

(a) Product - OPIP

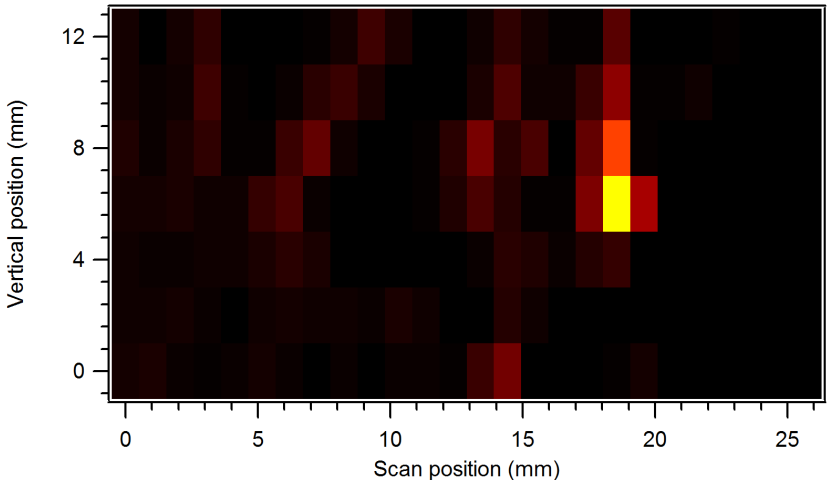

(b) Surface map - OPIP

Figure 10: Product of the OP and IP magnitude data, showing a notable improvement of the S/N ratio (a), plus the surface plot that shows the presence of both SCCs on sample A.

has been shown to be capable of detecting and locating real stress corrosion cracks contained in stainless steel pipe sections. The laser detection approach has the advantage that both detector and source have a very small spatial footprint on the sample surface, thereby allowing for the resolution of defects that are close together, as in sample A (figure 4b), where defects are spaced by a few mm, or close to the sample edges, as in sample B (figure 5b). This highlights the advantages of a laser-laser near-field approach, as the defects imaged would be very difficult to resolve from the backwall signal for reflection based techniques.

The EMAT detection approach has the advantage of reduced cost when compared to the laser interferometer, and EMATs are more easily implemented than the laser detection approach. With the information from the in-plane and out-of-plane data, access to information about the interaction of extra wavemodes with the SCC is available. The EMAT approach has some disadvantages, such as the reduced sensitivity, large spatial footprint and less clear interpretation of the data. However, the laser-laser measurements can be used to inform the results of the EMAT measurements, with EMATs used for practical implementation.

This technique shows promise with regards to characterising the defect geometry. Results presented here measure the spatial extent of the defect at the surface of the sample, with the level of enhancement observed related to the sample geometry [23, 24]. Measurements of machined simulated defects on plates using the analysis presented here has shown that, as the defect depth increases, so does the level of enhancement [24], and this has also been observed recently using SCC-type defects grown to different depths. When using Rayleigh waves, it has been shown that the enhancement is also sensitive to the angle of propagation of the defect into the sample, with the in-plane and out-of-plane enhancement used for characterisation [23]. Furthermore, once a defect is detected, the arrival times of the reflected wavemodes can be used to identify geometry, and potentially detect branching of the defect [35]. Combined with this detection using the signal enhancement, full defect characterisation is feasible.

The technique has the limitation of requiring access to the pipe surface, and is sensitive primarily to surface-breaking defects. We have presented measurements of the outer surface of pipes, however, measurement of defects on the inner surface is possible through using

pipeline pigging. A full measurement of the pipe, including internal defects, is then possible through a combination of this and other NDE techniques.

5. Acknowledgments

This work was funded by the European Research Council under Starting Independent Researcher Grant 202735, NonContactUltrasonic.

References

[1] R. Cottis, Stress corrosion cracking, Tech. rep., The National Physical Laboratory (2000).

[2] B. Larson, Study of the factors affecting the sensitivity of liquid penetrant inspections: Review of literature published from 1970 to 1998, Tech. rep., Center for aviation systems reliability (2002).

[3] P. Shull, Nondestructive evaluation. Theory, techniques and applications, CRC Press, 2002.

[4] H. Shaikh, N. Sivaibharasi, B. Sasi, T. Anita, R. Armirthalingam, B. Rao, T. Jayakumar, H. Khatak, B. Raj, Use of eddy current testing method in detection and evaluation of sensitisation and intergranular corrosion in austenitic stainless steels, Corrosion Science 48 (2006) 1462–1482.

[5] N. Yusa, S. Perrin, K. Mizuno, Z. Chen, K. Miya, Eddy current inspection of closed fatigue and stress corrosion cracks, Measurement Science and Technology 18 (2007) 3403–3408.

[6] T. Chen, G. Tian, A. Sophian, P. Que, Feature extraction and selection for defect classification of pulsed eddy current NDT, NDT&E International 41 (6) (2008) 467–476.

[7] S. Casalta, G. Daquino, L. Metten, J. Oudaert, A. V. de Sande, Digital image analysis of X-ray and neutron radiography for the inspection and the monitoring of nuclear materials, NDT&E International 36 (5) (2003) 349–355.

[8] L. Babout, T. Marrow, D. Engelberg, P. Withers, X-ray microtomographic observation of intergranular stress corrosion cracking in sensitised austenitic stainless steel, Materials Science and Technology 22 (2006) 1068–1075.

[9] D. Horner, B. Connolly, S. Zhou, L. Crocker, A. Turnbull, Novel images of the evolution of stress corrosion cracks from corrosion pits, Corrosion Science 53 (2011) 3466–3485.

[10] P. Petcher, S. Dixon, Wideband ultrasonic time of flight diffraction combining b scans and cross sectional imaging, in: AIP Conference proceedings 1096, 2009, pp. 650–657.

[11] P. Petcher, S. Dixon, Parabola detection using matched filtering for ultrasound b-scans, Ultrasonics 52 (2012) 138–144.

[12] A. K. Kromine, P. A. Fomitchov, S. Krishnaswamy, J. D. Achenbach, Laser ultrasonic detection of surface breaking discontinuities: Scanning laser source technique, Materials Evaluation 58 (2) (2000) 173–177.

[13] J. Blackshire, S. Sathish, Near-field ultrasonic scattering from surface-breaking cracks, Applied Physics Letters 80 (18) (2002) 3442–3444.

[14] I. Arias, J. Achenbach, A model for the ultrasonic detection of surface-breaking cracks by the scanning laser source technique, Wave Motion 39 (1) (2004) 61–75.

[15] R. S. Edwards, S. Dixon, X. Jian, Depth gauging of defects using low frequency wideband Rayleigh waves, Ultrasonics 44 (2006) 93–98.

[16] Y. Fan, S. Dixon, R. S. Edwards, X. Jian, Ultrasonic surface wave propagation and interaction with surface defects on rail track head, NDT&E International 40 (2007) 471–477.

[17] X. Jian, S. Dixon, N. Guo, R. Edwards, Rayleigh wave interaction with surface-breaking cracks, Journal of Applied Physics 101 (2007) 064906.

[18] S. Dixon, B. Cann, D. Carroll, Y. Fan, R. Edwards, Non-linear enhancement of laser generated rayleigh waves by cracks, Nondestrutive Testing and Evaluation 23 (2008) 25–34.

[19] A. Clough, R. Edwards, Scanning laser source lamb wave enhancements for defect characterisation., NDT&E International Under review (2013) NA.

[20] H. Xiao, P. Nagy, Enhanced ultrasonic detection of fatigue cracks by laser-induced crack closure, Journal of Applied Physics 83 (1998) 7453–7460.

[21] B. Dutton, A. Clough, M. Rosli, R. Edwards, Non-contact ultrasonic detection of angled surface defects, NDT&E International 44 (2011) 353–360.

[22] B. Dutton, A. Clough, R. Edwards, Near field enhancements from angled surface defects; a comparison of scanning laser source and scanning laser detection techniques, Journal of Nondestructive Evaluation 30 (2011) 64–70.

[23] M. Rosli, R. Edwards, Y. Fan, In-plane and out-of-plane measurements of rayleigh waves using emats for characterising surface cracks, NDT&E International 49 (2012) 1–9.

[24] A. Clough, R. Edwards, Lamb wave near field enhancements for surface breaking defects in plates, Journal of Applied Physics 111 (2012) 104906.

[25] S. E. Burrows, B. Dutton, S. Dixon, Laser generation of lamb waves for defect detection: Experimental methods and finite element modelling, IEEE Transactions on ultrasonics, ferroelectrics and frequency control 59 (2012) 82–89.

[26] J. Rose, Ultrasonic waves in solid media, Cambridge University Press, 1999.

[27] S. Palmer, S. Dixon, Industrially viable non-contact ultrasound, Insight 45 (2003) 211–217.

[28] C. B. Scruby, L. E. Drain, Laser ultrasonics. Techniques and applications, Adam Hilger, 1990.

[29] M. Klein, G. Bacher, A. Grunnet-Jepsen, D. Wright, W. E. Moerner, Homodyne detection of ultrasonic surface displacements using two-wave mixing in photorefractive polymers, Optics Communications 162 (1999) 79 – 84.

[30] M. Niethammer, L. Jacobs, J. Qu, J. Jarzynski, Time-frequency representations of lamb waves, Journal of the Acoustical Society of America 109 (5) (2001) 1841–1847.

[31] S. Dixon, S. Burrows, B. Dutton, Y. Fan, Detection of cracks in metal sheets using pulsed laser generated ultrasound and emat detection, Ultrasonics 51 (1) (2011) 7–16.

[32] K. Kawashima, Quantitative calculation and measurement of longitudinal and transverse ultrasonic wave pulses in solid, IEEE Transactions on sonics and ultrasonics 31 (2) (1984) 83–93.

[33] S. Dixon, C. Edwards, S. Palmer, High-accuracy non-contact ultrasonic thickness gauging of aluminium sheet using electromagnetic acoustic transducer, Ultrasonics 39 (2001) 445–453.

[34] M. Rosli, R. Edwards, B. Dutton, C. Johnson, P. Cattani, Identifying surface angled cracks on aluminium bar using emats and automated computer system, in: D. Thompson, D. Chimenti (Eds.), Review of progress in quantitative nondestructive evaluation, Vol. 29, Vol. AIP Conf. Proc. 1211, 2009, pp. 1593–1600.

[35] F. Hernandez-Vale, A. Clough, R. Edwards, to be published.